

1  
2  
3 The Distinct Behaviors of Pacific and Indian Ocean Warm Pool  
4 Properties on Seasonal and Interannual Timescales  
5  
6  
7

8 Seon Tae Kim and Jin-Yi Yu  
9

10 Department of Earth System Science  
11 University of California  
12 Irvine, California, 92697, USA  
13  
14

15 Mong-Ming Lu

16 Research and Development Center  
17 Central Weather Bureau  
18 Taipei 10048, Taiwan  
19  
20  
21

22 January 2012, Accepted

23 *Submitted to Journal of Geophysical Research-Atmospheres*  
24  
25  
26  
27  
28  
29  
30  
31  
32  
33

34  
35 

---

*Corresponding author address:* Seon Tae Kim, Department of Earth System Science,  
36 University of California, Irvine, California, 92697, USA, E-mail: seontk@uci.edu

## Abstract

37

38

39

The seasonal and interannual variability of warm pool properties in the Pacific and Indian Ocean sectors are examined and contrasted. The properties examined are the size, mean and maximum sea surface temperatures (SSTs), and central position. The seasonal variability is more vigorous in the Indian Ocean sector, but the interannual variability is comparable in the Pacific and Indian Ocean sectors. The variability is associated with significant longitudinal and latitudinal displacements on seasonal timescales but only with longitudinal displacements on interannual timescales. As for the controlling factors, while the seasonal variability of the warm pool is controlled by the annual march of the Sun in the Pacific sector and by the Indian summer monsoon in the Indian Ocean sector, the interannual variability in both sectors is related mostly to El Niño-Southern Oscillation (ENSO). ENSO is closely correlated with the size variations and longitudinal displacements of the warm pool. Interestingly, the warm pool intensity in both sectors is not highly correlated with ENSO until five to six months after ENSO peaks. The possible causes of this delayed ENSO influence are discussed. Only size and intensity (i.e., mean SST) variations in the Indian Ocean warm pool are significantly correlated with quasi-biennial variability in the Indian monsoon, which indicates that the Indian Ocean warm pool may be a potential predictor for Indian monsoon variations.

56 **1. Introduction**

57           The Indo-Pacific warm pool is an important feature of the climate system and is  
58 typically defined as the region of ocean enclosed by the 27.5°C or 28°C isotherm of sea  
59 surface temperature (SST) (e.g., Wyrski 1989; Ho et al. 1995; Fasullo and Webster 1999)  
60 which are threshold temperatures required for atmospheric deep convection (e.g., Graham  
61 and Barnett 1987; Zhang 1993; Fu et al. 1994). Through the excitement of deep  
62 convection, the warm pool is capable of influencing global climate via, for example, the  
63 Walker and Hadley circulations and serves as a major source of heat and water vapor  
64 (Sardekukh and Hoskins 1988; Webster and Lukas 1992). Variations in the properties of  
65 the warm pool have been considered as a driving force to, as well as an indication of,  
66 climate variability and changes. For example, the warm pool size was suggested to be a  
67 key factor regulating tropical mean SSTs by Pierrehumbert (1995). The extension of the  
68 warm pool is positively correlated with the occurrence of westerly wind bursts in the  
69 western Pacific, which are known to be important for the onset of the El Niño events  
70 (Eisenman et al. 2005). Warm pool displacements and intensity variations are also known  
71 to affect the onset, intensity, and period of El Niño-Southern Oscillation (ENSO) (Picaut  
72 et al. 1996; Kessler 2001; Sun 2003; McPhaden 2004). Changes in the warm pool size  
73 have been suggested to change the center of atmospheric deep convection, leading to  
74 local and remote changes in climate. Williams and Funk (2011) showed that a large  
75 warming trend in the Indian Ocean over the past 60 years has expanded the Indian Ocean  
76 warm pool westward and argued that this expansion has been instrumental in a shift of  
77 the sinking branch of the Walker circulation westward to eastern Africa, causing rainfall  
78 deficit there. It has also been suggested that warm pool SSTs may affect tropical cyclone  
79 frequency and intensity. Webster et al. (2005) showed that an increasing trend in the

80 tropical cyclone number and intensity over the past 35 years could be associated with a  
81 warming trend in the north Indian Ocean and western Pacific Ocean. Slow fluctuations in  
82 warm pool SSTs were suggested to be capable of regulating decadal variability in the  
83 Hadley and Walker circulations (Wang and Metha 2008). Furthermore, the warming of  
84 the Indo-Pacific warm pool in recent decades was suggested as a contributor to a trend of  
85 intensification in the Hadley circulation (Ma and Li 2008).

86

87         Previous studies have improved our understanding of the Indo-Pacific warm pool,  
88 such as its surface energy balance and the relative roles played by atmospheric and  
89 oceanic processes in the balance (e.g., Ramanathan and Collins 1991; Wallace 1992;  
90 Hartmann and Michelson 1993; Schneider et al. 1996; Fasullo and Webster 1999;  
91 Clement et al. 2005). Most of the studies focused on the Pacific sector of the warm pool.  
92 Some of the studies that looked into the Indian Ocean sector of the warm pool indicated  
93 that the surface energy balance in this sector differs from that in the Pacific sector.  
94 Schneider et al. (1996) concluded from an examination of coupled atmosphere-ocean  
95 model simulations that, on seasonal timescales, the solar penetration process affects the  
96 vertical temperature structure more in the Pacific than in the Indian Ocean. Fasullo and  
97 Webster (1999) found that the warm pool SST in the Indian Ocean is less sensitive to  
98 surface thermal forcing than it is in the Pacific. The warm pool in the Indian Ocean sector  
99 also has a stronger annual cycle than in the Pacific sector (Fasullo and Webster 1999).  
100 The warming trend in the warm pool since the 1970s has been about two to three times  
101 larger in the Indian Ocean sector than in the Pacific sector (Williams and Funk 2011).  
102 Coincident with the warming in the Indian Ocean, the mean strength of the Indian  
103 monsoon has weakened but its interannual variability has increased (Goswami 2005). It

104 was also noted that the typical negative correlation between ENSO and the Indian  
105 monsoon has weakened in recent decades (Kumar et al. 1999; Kinter et al. 2002). It has  
106 also been shown that the Indian Ocean warm pool is shallower than the Pacific warm  
107 pool (e.g., Meng and Wu 2002). Moreover, the Indian Ocean exhibits a unique  
108 interannual variability, which is called the Indian Ocean Dipole (IOD; Saji et al. 1999;  
109 Webster et al. 1999), that may interfere with the Indian Ocean sector of the warm pool.  
110 These studies indicated that the warm pool properties and their variability in the Pacific  
111 and Indian Ocean sectors can be different and may play different roles in the climate  
112 system.

113

114 In this study, we separate the Indo-Pacific warm pool into a Pacific sector and an  
115 Indian Ocean sector to examine and contrast their seasonal and interannual variability.  
116 We focus on variations in the warm pool intensity, size, and location. The warm pool  
117 intensity is often represented by the mean SST within the region where SSTs are greater  
118 than or equal to a threshold (which is usually set to be 28°C). Additionally, we also  
119 examine variations in the maximum SST inside the warm pool to see whether it is a good  
120 indicator of warm pool intensity. As for the warm pool location, previous studies have  
121 focused on the longitudinal displacement or the eastern boundary movement of the  
122 Pacific warm pool due to its close relation with the evolution of ENSO (e.g., Picaut et al.  
123 1996). In this study, we examine the movement of the center of the warm pool by  
124 examining both its longitudinal and latitudinal displacements. This so-called “centroid”  
125 movement of the warm pool has been examined by Ho et al. (1995) using a short period  
126 (1982-1992) of satellite data, but that study focused only on the Pacific sector of the  
127 warm pool. For the size variations of the warm pool, we focus on its horizontal surface

128 area, since a previous study by Meng and Wu (2002) showed that volume variations in  
129 both the Pacific and Indian Ocean sectors of the warm pool are similar to their surface  
130 area variations. Therefore, five particular properties of the warm pool are examined in  
131 this study: the horizontal size of the warm pool, the mean and maximum SSTs inside the  
132 warm pool, and the central longitudinal and latitudinal locations of the warm pool.

133

## 134 **2. Data set and method**

135 The SST dataset used in this study is the National Oceanic and Atmospheric  
136 Administration (NOAA) Extended Reconstruction of Historical Sea Surface Temperature  
137 version 3 (ERSST v3; Smith et al. 2008) from the National Climate Data Center (NCDC).  
138 The data is available from 1854 to 2011 on  $2^{\circ}\times 2^{\circ}$  grids and is produced by applying  
139 statistical methods to in situ and satellite observations. To test the sensitivity of the results  
140 to the SST dataset used, we also examine the Met Office Hadley Centre Sea Ice and Sea  
141 Surface Temperature data set (HadISST; Rayner et al. 2003), which is reconstructed using  
142 an empirical orthogonal function and reduced-space optimal interpolation (Kaplan et al.  
143 1998) and is available on  $1^{\circ}\times 1^{\circ}$  grids from 1871 to 2011. We found the results to be  
144 similar and present only those produced from the ERSST dataset here.

145

146 Using SST data for the period 1950-2010, the size, maximum and mean SSTs, and  
147 the longitudinal and latitudinal locations of the center of the warm pool are calculated in  
148 the region enclosed by the  $28^{\circ}\text{C}$  isotherm within the region between  $30^{\circ}\text{S}$ - $30^{\circ}\text{N}$  and  
149  $30^{\circ}\text{E}$ - $130^{\circ}\text{W}$ . We repeated our analyses with the warm pool defined by the  $27.5^{\circ}\text{C}$   
150 isotherm, which has been used in some studies (e.g., Graham and Barnett 1987) to define

151 warm pool, but found little difference. Only the results with the warm pool defined by the  
152 28°C isotherm are shown. In this study, the warm pool is separated into Pacific and  
153 Indian Ocean sectors (see Figure 2) based on the basin mask information from NOAA's  
154 National Oceanographic Data Center World Ocean Atlas 2009 (Locarnini et al. 2010).  
155 The boundary (i.e., the red-dashed line in Fig. 2) of the two sectors connects the  
156 Indonesian island chain from the southern tip of the Indo-China Peninsula to the northern  
157 tip of the Australia. For the sake of discussion, these two sectors are referred to,  
158 respectively, as the Indian Ocean warm pool and the Pacific warm pool. The central  
159 latitudinal and longitudinal locations of the warm pool are calculated using the following  
160 methods:

$$161 \quad X_{\text{center}} = \sum_{i=1}^n x_i/n \text{ and } Y_{\text{center}} = \sum_{i=1}^n y_i/n,$$

162 where  $x$  and  $y$  are, respectively, the longitudinal and latitudinal locations of SST data  
163 grids inside the region enclosed by the 28°C isotherm, and  $n$  is the total number of grid  
164 points inside the warm pool. Latitudinal weighting (i.e., the squared root of  $\cos(\text{latitude})$ )  
165 is considered in the calculation of the central locations.

166

167 To examine the relationship between the warm pool properties and the Indian  
168 monsoon for the period 1950-2010, we use the All-India Rainfall (AIR; Parthasarathy et  
169 al. 1994) index for the period 1950-2010 to examine the monsoon-warm pool  
170 relationships. The AIR, which is available from 1871 onwards, was compiled by the  
171 Indian Institute of Tropical Meteorology using an area-weighted surface rainfall data set  
172 from 306 stations within India.

173

### 174 **3. Seasonal variations of the warm pool properties**

175 We first examine how the Indo-Pacific warm pool moves between the Pacific and  
176 Indian Ocean sectors during its seasonal evolution. Figure 1 shows the respective  
177 percentages of the surface area of the warm pool within each of the sectors. It shows that  
178 the Pacific sector is always the dominant part of the warm pool throughout the year, but  
179 the warm pool moves more into the Pacific Ocean during boreal summer and more into  
180 the Indian Ocean during boreal spring. In August, the Pacific sector comprises 80% of the  
181 Indo-Pacific warm pool while the Indian Ocean sector comprises only 20%. In March, as  
182 much as 45% of the warm pool is located within the Indian Ocean. The variations in the  
183 area percentage are further examined using the monthly climatology of the warm pool  
184 SSTs in Figure 2. In both sectors, the warm pool moves northward during boreal summer  
185 and southward during boreal winter, following the annual march of the Sun. The Pacific  
186 warm pool reaches its largest size when it is at its northernmost latitude near the end of  
187 the boreal summer (September; Fig. 2i) and its smallest size when it is at its southernmost  
188 latitude near the end of boreal winter (February; Fig. 2b). Although similar latitudinal  
189 excursions occur in the Indian Ocean, the size variations in this sector are larger than  
190 those in the Pacific sector and differ in their evolution. Instead of having a maximum size  
191 in boreal summer as in the Pacific sector, the warm pool in the Indian Ocean sector is  
192 smallest in August-September. This is related to the fact that the Indian Ocean is uniquely  
193 bounded to the north by the Asian continents, which adds the Indian monsoon as an  
194 additional factor controlling the Indian Ocean warm pool size. The southwesterly  
195 monsoon during boreal summer induces coastal upwelling and enhances surface  
196 evaporation cooling in the western Arabian Sea, thereby shrinking the warm pool to a  
197 small area in the northeastern corner of the Indian Ocean (Figs. 2g-i). This is the time that

198 the Indian Ocean sector constitutes the smallest percentage of the Indo-Pacific warm pool  
199 in Fig. 1. It is during the two inter-monsoon seasons (i.e., boreal spring and autumn) that  
200 the Indian Ocean warm pool has relatively large size. Particularly in boreal spring, the  
201 warm pool covers most of the northern Indian Ocean, and the percentage of the warm  
202 pool in the Indian Ocean sector reaches its maximum value (Fig. 1). The seasonal  
203 variations shown in Figs. 1 and 2 suggest that the seasonal displacement of the warm pool  
204 between the Pacific and Indian Oceans is controlled by two factors: the annual march of  
205 the solar heating and the Indian summer monsoon.

206

207 We examine in Figures 3a-e the seasonal variations of five warm pool properties:  
208 horizontal size, latitudinal and longitudinal position, mean SST, and maximum SST.  
209 Values shown are the deviations from the respective annual means. Harmonic analyses  
210 are applied to the variations (shown in Figs. 3f-j) to determine whether the variations are  
211 dominated by the annual or semi-annual harmonics. Figures 3a and f indicate that the size  
212 variations of the warm pool (as a percentage of the annual mean) in both the Pacific and  
213 Indian Ocean sectors are dominated by the annual harmonics, consistent with the  
214 discussion in connection with Fig. 2, but due to differences in the phase of these two  
215 annual harmonics, the size variation of the entire Indo-Pacific warm pool is dominated by  
216 semi-annual harmonics. The Indo-Pacific warm pool expands to its maximum size in  
217 April when the Indian Ocean sector of the warm pool reaches its largest size and its  
218 secondary maximum in October when the Pacific sector reaches its maximum size. The  
219 Indo-Pacific warm pool contracts to its smallest size in January when the Pacific warm  
220 pool is at its smallest. The secondary minimum of the Indo-Pacific warm pool occurs in  
221 August when the Indian Ocean warm pool is at its smallest due to the summer monsoon-

222 induced cooling, which is partially compensated for by the expanding Pacific warm pool.  
223 It is obvious from Fig. 3a that the seasonal size variations of the Indo-Pacific warm pool  
224 follow more closely with the size variations in the Indian Ocean sector than with the  
225 variations in the Pacific sector.

226

227         The seasonal displacements in longitude and latitude of the center of the warm  
228 pool are shown in Figs. 3b-c, where positive (negative) deviations represent eastward  
229 (westward) or northward (southward) displacements from the annual-mean locations. The  
230 most obvious feature in Fig. 3c is that the warm pool migrates northward from boreal  
231 winter to summer and southward from boreal summer to winter in both the Pacific and  
232 Indian Ocean sectors. The displacements are overwhelmingly dominated by the annual  
233 harmonics (Fig. 3h) and are almost identical in amplitude in the two sectors (about  $\pm 7^\circ$ ),  
234 although the northward displacement in the Indian Ocean during summer is limited by  
235 the Asian continent. Figures 3b and g show that the longitudinal displacement of the  
236 warm pool is also dominated by the annual harmonics in both the Pacific and Indian  
237 Ocean sectors; however the displacements are in opposite directions. The warm pool in  
238 the Indian Ocean displaces westward as it expands in boreal spring and displaces  
239 eastward as it shrinks in boreal summer. As for the Pacific sector, the warm pool  
240 displaces eastward during boreal winter and spring, which is related to the eastward  
241 expansion of the southern branch of the Pacific warm pool during the austral summer as  
242 shown in Fig. 2. The southern branch retreats westward toward the Dateline by the end of  
243 austral winter (i.e., August). Figure 3b indicates that the longitudinal displacement of the  
244 warm pool is dominated by the boreal seasonal cycle (i.e., the Indian monsoon) in the  
245 Indian Ocean sector but by the austral seasonal cycle in the Pacific sector. In both sectors,

246 the center of the warm pool displaces about  $\pm 8^\circ$  in longitude during the course of the  
247 year. The longitudinal variations of the Indo-Pacific warm pool follow more closely those  
248 of the Indian Ocean sector, due to the larger size variations in this sector.

249

250         Next we examine the seasonal variations in the warm pool intensity. We focus on  
251 two quantities: the mean SST (Fig. 3d) and the maximum SST (Fig. 3e) within the warm  
252 pool. The annual-mean values of the mean SST in the Pacific ( $28.9^\circ\text{C}$ ) and Indian Ocean  
253 ( $28.7^\circ\text{C}$ ) sectors of the warm pool are almost the same. The mean SST in the Pacific  
254 sector varies little throughout the year (Fig. 3d) and is dominated by a weak semi-annual  
255 harmonic (Fig. 3i). The peak values occur in boreal spring and autumn when the Sun is  
256 directly overhead at the equator. In contrast, the mean warm-pool SST in the Indian  
257 Ocean sector experiences a relatively large seasonal variation with a maximum excursion  
258 of more than  $0.5^\circ\text{C}$ . The variation is dominated by an annual harmonic with the largest  
259 deviation in April, which is the time when the Indian Ocean warm pool expands to its  
260 maximum size (see Fig. 3a). The mean SST in this sector decreases from July to  
261 December, which also coincides with the period of time when the Indian Ocean warm  
262 pool shrinks. Seasonal variations in the warm-pool size and intensity (i.e., mean SST) are  
263 positively correlated in the Indian Ocean sector, with a correlation coefficient of 0.67 that  
264 is significant at a 95% level according to a student t-test. No such a significant positive  
265 correlation is found in the Pacific warm pool (the correlation coefficient is 0.43). The  
266 seasonal variations of the mean SST in the Indo-Pacific warm pool follow those of the  
267 Indian Ocean warm pool. As indicated in Fig. 3j, the maximum values of the warm pool  
268 SST in both the Pacific and Indian Ocean sectors are dominated by the semi-annual  
269 harmonics, with the peak values occurring near the boreal late spring and early winter,

270 which reflects the influence from the annual march of the solar heating and indicates that  
271 the maximum SST values of the warm pool are not well linked to the other four warm  
272 pool properties on seasonal timescales.

273

274 The analyses presented in Fig. 3 together indicate that the seasonal variability of  
275 warm pool size and intensity is more vigorous in the Indian Ocean sector than in the  
276 Pacific sector, while the longitudinal and latitudinal displacements of the warm pool are  
277 comparable in the two sectors. The standard deviations of the seasonal cycle shown in  
278 Figures 4a-e lend further support to this conclusion. The standard deviation of the size  
279 variation is about 30% for the Indian Ocean sector but only 11% for the Pacific sector,  
280 which is a statistically significant difference at the 95% level based on F-test. The  
281 differences between the two sectors in the seasonal variability of the mean SST and the  
282 maximum SST of the warm pool are also statistically significant. The seasonal variations  
283 in the warm pool size, intensity, and longitudinal displacement in the Indian Ocean sector  
284 are closely linked to each other by the monsoon: the stronger the warm pool intensity, the  
285 larger the warm pool size, and the greater the westward expansion of the warm pool. In  
286 contrast, the intensity of the Pacific warm pool varies little throughout the year, although  
287 the center of the Pacific warm pool undergoes seasonal variations comparable to those of  
288 the Indian Ocean warm pool. These contrasting features indicate the warm pool SST is  
289 more strongly regulated by dynamical and thermodynamical processes (e.g., Clement et  
290 al. 2005; Ramanathan and Collins 1991) in the Pacific sector than in the Indian Ocean  
291 sector.

292

293 **4. Interannual variations of the warm pool properties**

294 We next examine the magnitudes of the interannual variability of the warm pool  
295 in the Pacific and Indian Ocean sectors. Interannual anomalies are obtained by applying a  
296 three-month running mean to the warm pool properties after their monthly climatology  
297 and trends are removed. We first compare the standard deviations of the interannual  
298 variations to those of the seasonal variations in Figure 4. Figure 4a shows that the  
299 interannual variability in the Pacific warm pool size is comparable to the seasonal  
300 variability, but the interannual variability in the Indian Ocean sector is less than half of its  
301 seasonal variability. The interannual variability in the warm pool size is now comparable  
302 in the two sectors. Figures 4b and c show that the interannual variability of the warm pool  
303 is associated with large longitudinal displacements but small latitudinal displacements in  
304 both sectors. The longitudinal displacement is particularly large in the Pacific sector.  
305 Figure 4d shows that the interannual variations of the Pacific warm pool are accompanied  
306 by significant variations in the mean SST, which is also different from its seasonal  
307 variations. The interannual variability in the mean SST of warm pool is comparable in the  
308 Pacific and Indian Ocean sectors. Figure 4e shows that the interannual variability of the  
309 maximum SST is also comparable in these two sectors. The comparisons presented in  
310 Fig. 4 indicate that although the Indian Ocean sector dominates the seasonal variability of  
311 the Indo-Pacific warm pool, the interannual variability in the Pacific and Indian Ocean  
312 sectors are comparable. Furthermore, while the warm pool variability is associated with  
313 both longitudinal and latitudinal displacements on seasonal timescales, the variability is  
314 associated only with longitudinal displacements on interannual timescales. It is important  
315 to note that, for the entire Indo-Pacific warm pool, the interannual variability is  
316 comparable to the seasonal variability in size, longitudinal displacement, mean SST, and

317 maximum SST. Only for the latitudinal displacement, is the interannual variability  
318 significantly smaller than the seasonal variability.

319

320         There are at least two possible contributors to interannual variability in the Indo-  
321 Pacific warm pool: ENSO and monsoon. We now look into their respective contributions  
322 to warm pool variability in each of the two ocean sectors. To investigate the relationship  
323 between the warm pool and ENSO, we display in Table 1 the correlation coefficients  
324 between monthly warm pool properties and the monthly Niño3.4 SST index (SST  
325 anomalies averaged in the region between 5°N-5°S and 170°W-120°W). The table shows  
326 that ENSO is significantly correlated (at the 95% level) with the size variations and  
327 longitudinal displacements of the Pacific warm pool. El Niño events increase the size of  
328 the Pacific warm pool and shift the center of the warm pool eastward, vice versa for La  
329 Niña events. ENSO accounts for about 63% of the interannual variability in warm pool  
330 size and about 78% of that in longitudinal displacement. We also calculate the correlation  
331 coefficients for boreal summer (July-August-September; JAS) and winter (December-  
332 January-February; DJF). As shown in Table 1, the correlations between Niño3.4 and  
333 warm pool size and longitudinal displacement are significant in both seasons. Since  
334 ENSO typically develops in summer and peaks in winter, Table 1 indicates that the  
335 significant correlations of ENSO with the warm pool size and longitudinal displacement  
336 persist throughout its lifecycle.

337

338         Table 1 also indicates that ENSO is not significantly correlated with interannual  
339 variations in the Pacific warm pool intensity (i.e., the mean and maximum SSTs). The  
340 weak correlation with the Pacific warm pool intensity can be understood by looking at the

341 typical SST anomaly pattern in the Indo-Pacific Ocean during ENSO events, as shown in  
342 Figure 5. This pattern is obtained by regressing Indo-Pacific SST anomalies with the  
343 Niño3.4 SST index for JAS and DJF. It is evident from the figure that while SSTs in the  
344 eastern half of the Pacific warm pool (the outline of the warm pool is indicated in Figs.  
345 5e-h by black counter) increase, there are negative SST anomalies in the western half of  
346 the Pacific warm pool. As a result of this partial cancellation, the warming effect of El  
347 Niño (or the cooling effect of La Niña) is not well reflected in the mean SST and  
348 maximum SST. It is noticed that the magnitude of the SST anomalies in the far western  
349 Pacific does not change much when the SST anomalies increase in the eastern-to-central  
350 Pacific during the development of the El Niño or La Niña event from JAS to DJF.  
351 Therefore, the cancellation effect is weaker in DJF when ENSO events peak. This is  
352 consistent with Table 1 that shows the mean SST in the warm pool has a significant  
353 correlation with ENSO in DJF.

354

355 Table 1 also shows that, although ENSO's correlation with the latitudinal  
356 displacement of the Pacific warm pool is not statistically significant for the entire  
357 calendar year, the correlation is significant in boreal summer. To further understand this  
358 correlation, we show in Figures 5e-h the outline of the seasonal warm pool and the  
359 outline of the warm pool corresponding to four standard deviations (STDs) of Niño3.4  
360 index. The four STDs are used in this figure to amplify the ENSO influences on the warm  
361 pool displacement. These figures show that while the Pacific warm pool expands and  
362 contracts during ENSO mainly via longitudinal displacements, the latitudinal profile of  
363 the warm pool surface does change. The change is particularly obvious in JAS during the  
364 time when the Pacific warm pool is located near the equator and both the northern and

365 southern branches of the warm pool (i.e., the warm waters that coincide, respectively,  
366 with the Inter-Tropical Convergence Zone and the South Pacific Convergence Zone) are  
367 influenced by ENSO. Between these two branches, the southern branch contains a larger  
368 surface area of warm water than the northern branch. The southern branch extends  
369 eastward during El Niño and retreats westward during La Niña. As a result, the  
370 percentage of the surface area of the warm pool in the southern branch increases during  
371 El Niño and decreases during La Niña. Therefore, the latitudinal center of the Pacific  
372 warm pool shifts southward during El Niño and northward during La Niña. This explains  
373 why Table 1 shows a significant negative correlation between the latitudinal displacement  
374 of the Pacific warm pool and ENSO in JAS. During DJF, the southern branch of the  
375 Pacific warm pool moves southward extending to 20°S and is less influenced by ENSO  
376 warming and cooling, and thus the weak correlation with the Niño3.4 index (see Table 1).

377

378         As for the Indian Ocean sector of the warm pool, Table 1 shows that ENSO has a  
379 remote influence on the size, intensity, and longitudinal displacement of the Indian Ocean  
380 warm pool with the correlation coefficients significant at 95% level. Particularly, the  
381 significant correlation with the intensity of the Indian Ocean warm pool is a distinctive  
382 feature that is not found for the Pacific warm pool. When the correlation is separately  
383 estimated for JAS and DJF, ENSO's correlations with the size and intensity of the Indian  
384 Ocean warm pool are significant in DJF (i.e., the peak phase of ENSO). We find from  
385 Figures 5c-d that the stronger winter correlations are related to a basin-wide warming and  
386 cooling of the Indian Ocean during the mature phase of ENSO events. It is known that  
387 the Indian Ocean tends to warm up (cool down) basin-wide after an El Niño (La Niña)  
388 event peaks due to the ENSO-induced heat flux anomalies (Klein et al. 1999) and ocean

389 Rossby wave propagation (Xie et al. 2002). This basin-wide warming/cooling typically  
390 peaks in late boreal winter and early spring and this explains why ENSO's correlation  
391 with the warm pool intensity is large and significant in DJF. The basin-wide warming  
392 (cooling) during El Niño (La Niña) expands (shrinks) the Indian Ocean warm pool and  
393 also explains why the size of the Indian Ocean warm pool is significantly correlated with  
394 the ENSO during DJF (see Table 1). The correlation analysis also indicates that the  
395 longitudinal displacement of the Indian Ocean warm pool due to ENSO is in an opposite  
396 direction from that of the Pacific warm pool with significant correlation persisting from  
397 the ENSO development to its peak. The opposite longitudinal displacement between the  
398 two sectors during ENSO can be attributed to the opposite directions of the Pacific and  
399 Indian Ocean branches of the global Walker circulation.

400

401 To further explore the cause-and-effect relations between ENSO and warm pool  
402 variations, their lead-lag correlations are calculated and shown in Figure 6. For the  
403 Pacific warm pool (Fig. 6a), the largest correlations occur when ENSO (i.e., the Niño3.4  
404 SST index) leads the warm pool size by one month. It is also noticed that about five  
405 months after ENSO reaches its mature stage the Pacific warm pool mean SST reaches its  
406 peak value. This may be the time when the SST anomalies in the western Pacific that are  
407 out-of-phase with the ENSO SST anomalies diminish. The longitudinal displacement of  
408 the Pacific warm pool occurs almost simultaneously with the development of the ENSO.  
409 As for the Indian Ocean sector (Fig. 6b), the warm pool is displaced to the west  
410 simultaneously during the ENSO development while the warm pool size reaches its peak  
411 two months after ENSO peaks. Figure 6b also shows that the mean SST of the Indian  
412 Ocean warm pool is affected remotely by ENSO with a lag time of four months. As

413 mentioned, the enhanced warm pool mean SST during El Niño is related to the Indian  
414 Ocean basin-wide warming, which is known to reach its maximum about one season after  
415 El Niño peaks (An 2004; Yu and Lau 2005). The El Niño-induced tropical Indian Ocean  
416 warming can persist through the spring and early summer after ENSO dissipates and can  
417 prolong ENSO's influence on the climate of the Indian and western Pacific region (e.g.  
418 Annamalai et al. 2005; Yang et al. 2007; Xie et al. 2009, 2010; Du et al., 2009, 2011).  
419 This so-called capacitor effect of the Indian Ocean may also explain the lagged response  
420 to ENSO of the mean SST in the Pacific and Indian Ocean sectors of the warm pool.

421

422 We also examine the relationship between the Indian monsoon and warm pool  
423 properties. Figures 7a-e displays the lead-lag correlations between the June-July-August  
424 (JJA) AIR index and the warm pool properties. The figure shows that the Indian monsoon  
425 rainfall is more highly correlated with the warm pool variability in the Indian Ocean  
426 sector (the black curves) than with that in the Pacific sector (the red curves). Correlations  
427 of the Indian monsoon with the Pacific warm pool are mostly not statistically significant  
428 at the 95% level. The size of the Indian Ocean warm pool has a positive correlation with  
429 the monsoon variability during the seasons preceding the summer monsoon and a  
430 negative correlation after the monsoon season (Fig. 7a). A similar lead-lag correlation is  
431 also found with the mean SST of the Indian Ocean warm pool (Fig. 7d). These relations  
432 indicate that a stronger-than-normal Indian summer monsoon is preceded by an  
433 expanding and warming Indian Ocean warm pool in boreal spring and followed by a  
434 shrinking and cooling Indian Ocean warm pool in boreal autumn. It is likely that the  
435 larger size and warmer Indian Ocean warm pool can supply more moisture into the Indian  
436 Peninsula to produce a stronger summer monsoon, thereby producing stronger surface

437 winds over the Indian Ocean, enhancing surface evaporation and acting to cool down the  
438 warm pool afterward. These cyclic feedback processes between the monsoon and the  
439 Indian Ocean warm pool take about two years, according to the interval between the  
440 largest positive and negative correlations shown in Fig. 7a and d. This result indicates  
441 that the correlation between the Indian Ocean warm pool and monsoon is strong on the  
442 biennial timescale, which is consistent with Li et al. (2001) who argued that the strength  
443 of the Indian monsoon is affected more by the Indian Ocean in the two-three year band  
444 but by ENSO on other interannual timescales. The cause of this strong biennial  
445 correlation may be the local monsoon-ocean interactions proposed as the source of the  
446 so-called Tropospheric Biennial Oscillation (TBO; Meehl 1987, 1993) or by remote  
447 influences from the biennial component of ENSO on both the monsoon and the Indian  
448 Ocean (Fasullo 2004).

449

450         Figures 7b and c show that size variations in the Indian Ocean warm pool are  
451 associated with both longitudinal and latitudinal displacements of the center of the warm  
452 pool although the correlations do not exceed the 95% significance level. Preceding a  
453 stronger-than-normal Indian summer monsoon, the Indian Ocean warm pool expands into  
454 the western (Fig. 7b) and northern (Fig. 7c) Indian Ocean. Conversely, after the strong  
455 monsoon, the warm pool retracts into the eastern and southern Indian Ocean. Also,  
456 summer monsoon rainfall is only weakly correlated with the maximum SST (Fig. 7e) in  
457 the Indian Ocean sector of the warm pool. Therefore, it is interesting to note that the  
458 Indian monsoon can affect the Indian Ocean warm pool intensity (i.e., mean SST) on both  
459 seasonal and interannual timescales. The biennial variability of the monsoon is closely  
460 correlated with the size and mean SST of the Indian Ocean warm pool.

461

462           We also looked into the lead-lag correlations between the warm pool properties  
463 and the IOD. Following Saji et al. (1999), an IOD index is defined as the difference in  
464 SST anomaly between the tropical western Indian Ocean (50°E-70°E, 10°S-10°N) and  
465 the tropical southeastern Indian Ocean (90°E-110°E, 10°S-0°). We found that the largest  
466 correlation coefficients (which are significant at the 95% level) occur when the IOD leads  
467 the size and the longitudinal location of Indian Ocean warm pool by about two to three  
468 months. The correlations (not shown) indicate that the Indian Ocean warm pool expands  
469 toward the west after a positive phase of the IOD and contracts toward the east after a  
470 negative phase of the IOD. No significant correlations are found with other properties of  
471 the Indian Ocean warm pool or properties of the Pacific warm pool. Apparently, the  
472 influence of the IOD is limited to the Indian Ocean warm pool despite the global climate  
473 impacts of the IOD that have been reported in several studies (e.g., Saji and Yamagata  
474 2003; Guan and Yamagata 2003).

475

476           Lastly, we examine in Fig. 8 the lead-lag correlations between the Pacific and  
477 Indian Ocean sectors of the warm pool. The figure shows that these two sectors are  
478 significantly correlated for the variations in size, longitudinal displacement, and intensity  
479 (both the mean SST and the maximum SST). The largest correlation coefficients occur  
480 when the size and the longitudinal displacement of the Pacific warm pool lead those of  
481 the Indian Ocean warm pool by three months. These correlations are consistent with the  
482 timing of the Pacific and Indian Ocean warm pool responses to ENSO as discussed  
483 previously (see Fig. 6). The warm pool intensity (e.g., mean and maximum SST) in both  
484 sectors varies almost simultaneously due to their similar delayed responses to ENSO

485 warming/cooling as discussed in connection with Fig. 6. Figure 8 shows that the  
486 interactions between the Pacific and Indian Ocean sectors of the warm pool are results of  
487 ENSO forcing.

488

## 489 **6. Summary and discussion**

490 This study examined the seasonal and interannual variations of five Indo-Pacific  
491 warm pool properties (size, mean and maximum SSTs, and latitudinal and longitudinal  
492 center) and contrasted the variability in the Pacific and Indian Ocean sectors. We  
493 conclude that variations in the warm pool are dominated by the Indian Ocean sector on  
494 seasonal timescales but that both sectors contribute significantly to the interannual  
495 variability. On seasonal timescales, the Pacific warm pool expands and contracts by only  
496 about 15% of its annual-mean size at the most, while the Indian Ocean warm pool varies  
497 in size by as much as 50%. The large variations in the Indian Ocean sector are related to  
498 strong local influences from the Indian summer monsoon. The size variations in both  
499 sectors are accompanied by large latitudinal displacements of the warm pool, which are  
500 controlled by the annual march of the Sun. The longitudinal displacements of the warm  
501 pool is not as large as the latitudinal displacements and are found to be controlled by the  
502 seasonal cycle of the monsoon in the Indian Ocean sector, and by the austral seasonal  
503 cycle in the Pacific sector.

504

505 On interannual timescales, the magnitude of the warm pool variability in the  
506 entire Indo-Pacific warm pool is similar to the magnitude of the seasonal variability. In  
507 contrast to the seasonal variability, the interannual variability is associated with large  
508 longitudinal displacements but small latitudinal displacements. ENSO is the primary

509 contributor to the interannual variability in both sectors. When an El Niño event  
510 develops, the size of the warm pool increases as it extends eastward in the Pacific sector  
511 and westward in the Indian Ocean sector, and vice versa for a La Niña event. This study  
512 finds that the response of the warm pool intensity to ENSO does not reach its peak until  
513 about five months after ENSO peaks. The delay in the Indian Ocean is due to the time  
514 required for ENSO-induced basin-wide warming/cooling to develop. The delay in the  
515 Pacific is due to an out-of-phase SST anomaly that develops in the western half of the  
516 Pacific warm pool that partially cancels out the warming (cooling) effects associated with  
517 El Niño (La Niña) events in the eastern half. This cancellation effect diminishes gradually  
518 about five to six months after ENSO peaks. Therefore, this study finds that the intensity  
519 of ENSO, which tends to peak in boreal winter, may be reflected in the Pacific or Indian  
520 Ocean warm pool intensity during the following boreal spring. Finally, the quasi-biennial  
521 variability of the Indian monsoon, which is known as the TBO, is also found to have  
522 strong interactions with the Indian Ocean warm pool. The positive phase of the TBO (i.e.,  
523 stronger-than-normal summer monsoon) is preceded by an expanding and warming  
524 Indian Ocean warm pool and followed by a shrinking and cooling warm pool. The  
525 correlation implies that the interannual variations in both size and mean SST in the Indian  
526 Ocean warm pool have the potential to be utilized for the prediction of Indian monsoon  
527 variations.

528

529         ***Acknowledgments*** The authors thank three anonymous reviewers for their  
530 valuable comments. JYY and STK acknowledge support from the NSF Climate and  
531 Large-Scale Dynamics program (ATM-0925396) and NOAA-MAPP Program

532 (NA11OAR4310102). MML acknowledges the support from National Science Council of  
533 Taiwan ROC (NSC 99-2625-M-052-002-MY3).

534 **References**

- 535 An, S.-I., 2004: A dynamic link between the basin-scale and zonal modes in the tropical  
536 Indian Ocean. *Theor. Appl. Climatol.*, **78**, 203-215.
- 537 Annamalai, H., S.-P. Xie, J.-P. McCreary, and R. Murtugudde, 2005: Impact of Indian  
538 Ocean sea surface temperature on developing El Niño. *J. Climate*, **18**, 302–319.
- 539 Clement, A. C., R. Seager, and R. Murtugudde, 2005: Why are there tropical warm pools?  
540 *J. Climate*, **18**, 5294-4331.
- 541 Du, Y., S.-P. Xie, G. Huang, K. Hu, 2009: Role of Air–Sea Interaction in the Long  
542 Persistence of El Niño–Induced North Indian Ocean Warming. *J. Climate*, **22**,  
543 2023–2038.
- 544 Du, Y., L. Yang, S.-P. Xie, 2011: Tropical Indian Ocean Influence on Northwest Pacific  
545 Tropical Cyclones in Summer following Strong El Niño. *J. Climate*, **24**, 315–322.
- 546 Eisenman, I., L. Yu, and E. Tziperman, 2005: Westerly wind bursts: ENSO’s tail rather  
547 than the dog? *J. Climate*, **18**(24), 5224–5238.
- 548 Fasullo, J., 2004: Biennial characteristics of Indian monsoon rainfall. *J. Climate*, **17**,  
549 2972-2982.
- 550 Fasullo, J., and P. J. Webster, 1999: Warm pool SST variability in relation to the surface  
551 energy balance. *J. Climate*, **12**, 1292-1305.
- 552 Fu, R., A. D. Del Genio, and W.B. Rossow, 1994: Influence of ocean surface conditions  
553 on atmospheric vertical thermodynamic structure and deep convection. *J. Climate*,  
554 **7**, 1092-1108.

- 555 Goswami, B. N., 2005: The Asian Monsoon: Interdecadal Variability: in The Global  
556 Monsoon System: Research and Forecast. Edited by C.-P. Chang, Bin Wang, Ngar-  
557 Cheung Gabriel Lau, Chapter 26, pp 455.
- 558 Graham, N. E., and Barnett T. P., 1987: Sea surface temperature, surface wind  
559 divergence, and convection over tropical oceans, *Science*, **238** (4827), 657-659.
- 560 Guan, Z., and T. Yamagata, 2003: The unusual summer of 1994 in East Asia: IOD  
561 teleconnections. *Geophys. Res. Lett.*, **30**, 1544, doi:10.1029/2002GL016831.
- 562 Hartmann, D. L., and M. L. Michelsen, 1993: Large-scale effects on the regulation of  
563 tropical sea surface temperature. *J. Climate*, **6**, 2049–2062.
- 564 Ho, C.-R., X.-H. Yan, and Q. Zheng, 1995: Satellite observations of upper-layer  
565 variabilities in the western Pacific warm pool. *Bull. Amer. Meteor. Soc.*, **76**, 669-  
566 679.
- 567 Kaplan, A., M. A. Cane, Y. Kushnir, A. C. Clement, M. B. Blumenthal, and B.  
568 Rajagopalan, 1998: Analyses of global sea surface temperature 1856–1991, *J.*  
569 *Geophys. Res.*, **103**, 18,567–18,589.
- 570 Kessler, W. S., 2001: EOF representations of the Madden–Julian oscillation and its  
571 connection with ENSO. *J. Climate*, **14**, 3055–3061.
- 572 Kinter III, J. L., K. Miyakoda, and S. Yang, 2002: Recent change in the connection from  
573 the Asian monsoon to ENSO. *J. Climate*, **15**, 1203-1215.
- 574 Klein, S. A., B. J. Soden, and N.-C. Lau, 1999: Remote sea surface temperature variations  
575 during ENSO: Evidence for a tropical atmospheric bridge. *J. Climate*, **12**, 917-932.

- 576 Kumar, K. K., B. Rajagopalan, and M. A. Cane, 1999: On the weakening relationship  
577 between the Indian Monsoon and ENSO. *Science*, **284**, 2156-2159.
- 578 Locarnini, R. A., A. V. Mishonov, J. I. Antonov, T. P. Boyer, H. E. Garcia, O. K.  
579 Baranova, M. M. Zweng, and D. R. Johnson, 2010: World Ocean Atlas 2009,  
580 Volume 1: Temperature. S. Levitus, Ed. NOAA Atlas NESDIS 68, U.S. Government  
581 Printing Office, Washington, D.C., 184 pp.
- 582 Li, T., Y. S. Zhang, C. P. Chang, and B. Wang, 2001: On the relationship between Indian  
583 Ocean SST and Asian summer monsoon. *Geophys. Res. Lett.*, **28**, 2843-2846.
- 584 Ma, J., and J. Li, 2008: The principal modes of variability of the boreal winter Hadley  
585 cell. *Geophys. Res., Lett.*, **35**, L01808, doi:10.1029/2007GL031883.
- 586 McPhaden, M. J., 2004: Evolution of the 2002/03 El Niño. *Bull. Amer. Meteor. Soc.*,  
587 **85**(5), 677–695.
- 588 Meehl, G. A., 1987: The annual cycle and interannual variability in the tropical Indian  
589 and Pacific Ocean regions. *Mon. Wea. Rev.*, **115**, 27-50.
- 590 Meehl, G. A., 1993: A coupled air-sea biennial mechanism in the tropical Indian and  
591 Pacific regions: Role of oceans. *J. Climate*, **6**, 31-41.
- 592 Meng, X., and D. Wu, 2002: Contrast between the climatic states of the warm pool in the  
593 Indian Ocean and in the Pacific Ocean. *J. Ocean. Univ. China.*, **1**, 119-124, doi:  
594 10.1007/s11802-002-0003-y
- 595 Parthasarathy B., A. A. Munot, and D.R. Kothawale, 1994: All India monthly and  
596 seasonal rainfall series: 1871-1993. *Theor. Appl. Climatol.*, **49**, 217-224.

597 Picaut, J., M. Ioualalen, C. Menkes, T. Delcroix, and M. J. McPhaden, 1996: Mechanism  
598 of the zonal displacements of the Pacific warm pool: Implications for ENSO.  
599 *Science*, **274**, 1486-1489.

600 Pierrehumbert, R. T., 1995: Thermostats, radiator fins, and the runaway greenhouse. *J.*  
601 *Atmos. Sci.*, **52**, 1784–1806.

602 Ramanathan, V., and W. Collins, 1991: Thermodynamic regulation of ocean warming by  
603 cirrus clouds deduced from observations of the 1987 El Niño. *Nature*, **351**, 27–32.

604 Rayner, N. A., D. E. Parker, E. B. Horton, C. K. Folland, L. V. Alexander, D. P. Rowell,  
605 E. C. Kent, and A. Kaplan, 2003: Global analyses of sea surface temperature, sea  
606 ice, and night marine air temperature since the late nineteenth century. *J. Geophys.*  
607 *Res.*, **108**, 4407, doi:10.1029/2002JD002670.

608 Saji, N. H., B. N. Goswami, P. N. Vinayachandran, and T. Yamagata, 1999: A dipole  
609 mode in the tropical Indian Ocean. *Nature*, **401**, 360–363.

610 Saji, N. H., and T. Yamagata, 2003: Possible impacts of Indian Ocean dipole mode events  
611 on global climate. *Climate Res.*, **25**, 151–169.

612 Sardeshmukh, P. D., and B. J. Hoskins, 1988: the generation of global rotational flow by  
613 steady idealized tropical divergence. *J. Atmos. Sci.*, **45**, 1228-1251.

614 Schneider, N., T. Barnett, M. Latif, and T. Stockdale, 1996: Warm pool physics in a  
615 coupled GCM. *J. Climate*, **9**, 219-239.

- 616 Smith, T. M., R. W. Reynolds, T. C. Peterson, and J. Lawrimore, 2008: Improvements to  
617 NOAA's Historical Merged Land-Ocean Surface Temperature Analysis (1880-  
618 2006). *J. Climate*, **21**, 2283-2296.
- 619 Sun, D.-Z., 2003: A possible effect of an increase in the warm pool SST on the magnitude  
620 of El Niño warming. *J. Climate*, **16**(2), 185–205.
- 621 Wallace, J. M., 1992: Effect of deep convection on the regulation of tropical sea surface  
622 temperature. *Nature*, **357**, 230–231.
- 623 Wang, H., and M. Metha, 2008: Decadal variability of the Indo-Pacific warm pool and its  
624 association with atmospheric and oceanic variability in the NCEP-NCAR and  
625 SODA reanalyses. *J. Climate*, **21**, 5545-5565.
- 626 Webster, P. J., and R. Lukas, 1992: TOGA COARE: The coupled ocean atmosphere  
627 response experiment. *Bull. Amer. Meteor. Soc.*, **73**, 1377-1416.
- 628 Webster, P. J., A. M. Moore, J. P. Loschnigg, and R. R. Leben, 1999: Coupled oceanic-  
629 atmospheric dynamics in the Indian Ocean during 1997–98. *Nature*, **401**, 356–360.
- 630 Webster, P. J., G. J. Holland, J. A. Curry, and H. R. Chang, 2005: Changes in tropical  
631 cyclone number, duration, and intensity in a warming environment. *Science*,  
632 **309**(5742), 1844–1846.
- 633 Williams, P., and C. Funk, 2011: A westward extension of the warm pool leads to a  
634 westward extension of the Walker circulation, drying eastern Africa. *Climate Dyn.*,  
635 **37**, 2417-2435, doi 10.1007/s00382-010-0984-y.

636 Wyrski, K., 1989: Some thoughts about the West Pacific Warm Pool, in: J. Picaut, et al.  
637 Eds., Proc. of Western Pacific International Meeting and Workshop on TOGA  
638 COARE. 99-109.

639 Xie, S.-P., H. Annamalai, F. A. Schott, and J. P. McCreary, 2002: Structure and  
640 mechanisms of South Indian Ocean climate variability. *J. Climate*, **15**, 864-878.

641 Xie, S.-P., K. Hu, J. Hafner, H. Tokinaga, Y. Du, G. Huang, and T. Sampe, 2009: Indian  
642 Ocean capacitor effect on Indo-western Pacific climate during the summer  
643 following El Niño. *J. Climate*, **22**, 730–747.

644 Xie, S.-P., Y. Du, G. Huang, X.-T. Zheng, H. Tokinaga, K. Hu, and Q. Liu, 2010: Decadal  
645 shift in El Niño influences on Indo-western Pacific and East Asian climate in the  
646 1970s. *J. Climate*, **23**, 3352-3368.

647 Yang, J., Q. Liu, S.-P. Xie, Z. Liu, and L. Wu, 2007: Impact of the Indian Ocean SST  
648 basin mode on the Asian summer monsoon. *Geophys. Res. Lett.*, **34**, L02708,  
649 doi:10.1029/2006GL028571.

650 Yu, J.-Y. and K. M. Lau 2005: Contrasting Indian Ocean SST variability with and without  
651 ENSO influence: A coupled atmosphere-ocean GCM study. *Meteorol. Atmos. Phys.*,  
652 **90**, 179-191, doi: 10.1007/s00703-004-0094-7.

653 Zhang, C., 1993: Large-scale variability of atmospheric deep convection in relation to sea  
654 surface temperature in the Tropics. *J. Climate*, **6**, 1898–1913.

655 **List of Figures**

656 Figure 1. The seasonal evolution of the percentages of the Indo-Pacific warm pool in the  
657 Pacific and Indian Ocean sectors.

658 Figure 2. The monthly climatology of the Indo-Pacific warm pool SSTs. Values shown  
659 are the monthly mean SSTs greater than 28°C; the threshold used to define the Indo-  
660 Pacific warm pool. The boundary between the Pacific and Indian Ocean sectors of the  
661 warm pool is indicated by a red dashed line.

662 Figure 3. The seasonal cycle (left panels) and its harmonics (right panels) of warm pool  
663 properties; (a, f) horizontal size, (b, g) the longitudinal displacement, (c, h) the latitudinal  
664 displacement, (d, i) mean SST, and (e, j) maximum SST. Thick-solid lines represent  
665 values for the Indo-Pacific warm pool, thin-dashed lines for the Pacific warm pool, and  
666 thin-solid lines for the Indian Ocean warm pool.

667 Figure 4. Standard deviations of seasonal (left) and interannual (right) variability of (a)  
668 horizontal size, (b) mean SST, (c) maximum SST, (d) the longitudinal displacement, and  
669 (e) the latitudinal displacement for the Pacific and Indian Ocean sectors and the total  
670 warm pool. Values of the standard deviations are shown in parentheses on top of the bars.

671 Figure 5. Spatial patterns of SST anomalies (left panels) and the warm pool (right  
672 panels). They are obtained separately for El Niño (a, c, e, g) and La Niña (b, d, f, h)  
673 phases and for JAS (a, b, e, f) and DJF (c, d, g, h) averaged values. The SSTA spatial  
674 patterns are produced by multiplying a four standard deviation (STD) of the Niño3.4  
675 index to the regression of the SSTA on the Niño3.4 SST index. The black 28°C isotherm

676 of SST represents the JAS and DJF climatology and the red isotherm the sum of the  
677 climatology and regressed SSTA multiplied by four STD.

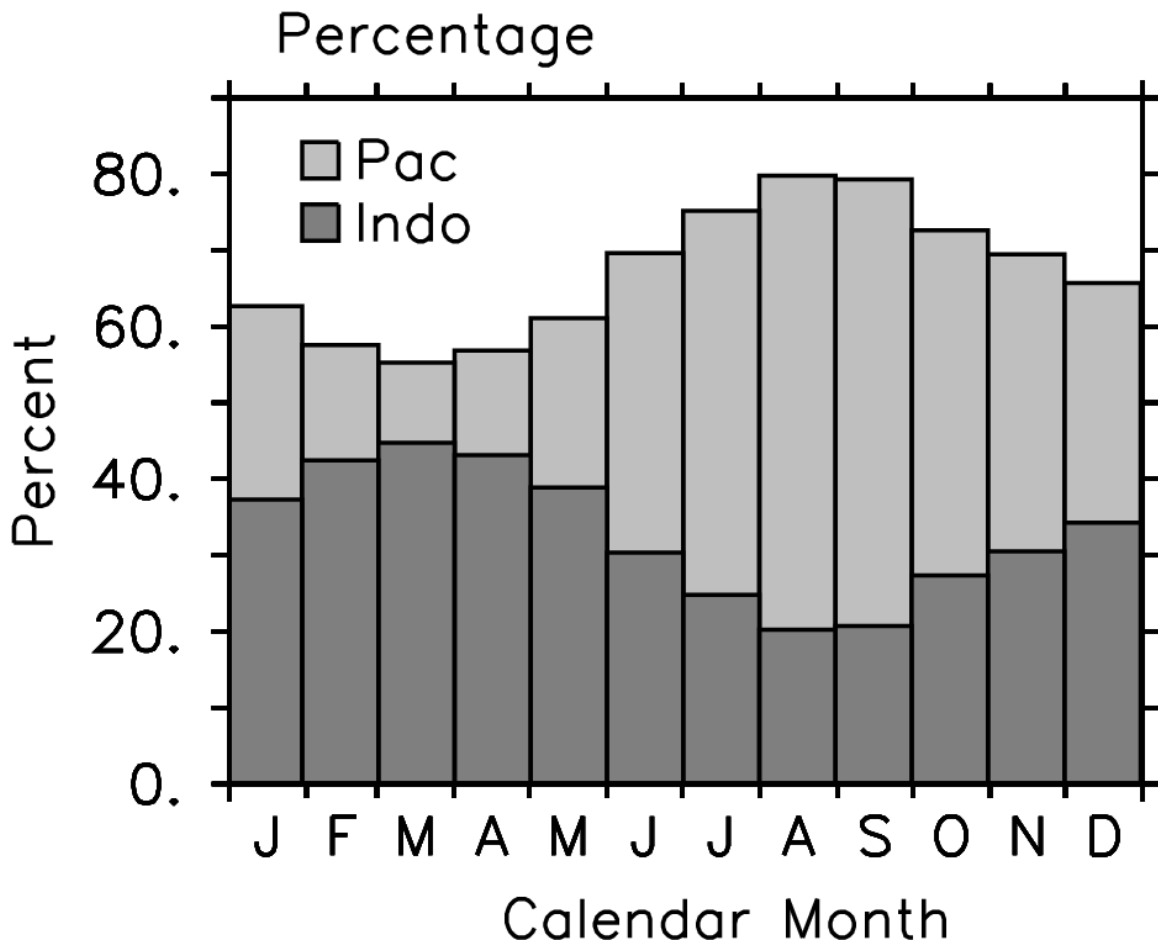
678 Figure 6. Lead-lag correlations between the Niño 3.4 indices and warm pool properties  
679 for (a) the Pacific sector and (b) the Indian Ocean sector on interannual timescales. The  
680 warm pool properties analyzed are the size (black), longitudinal displacement (red), and  
681 mean SST (green). Positive lags indicate that the ENSO leads the warm pool properties.  
682 Correlations significant at the 95% confidence level are indicated by the horizontal  
683 dashed lines.

684 Figure 7. Correlations of the June-July-August All India rainfall (AIR) index with the  
685 warm pool properties: (a) size, (b) longitudinal displacement, (c) latitudinal displacement,  
686 (d) mean SST, and (e) maximum SST of the Pacific (red) and Indian Ocean (black) warm  
687 pool. Correlations significant at the 95% confidence level are indicated by the horizontal  
688 dashed lines.

689 Figure 8. Lead-lag correlations of warm pool properties in the Pacific and Indian Ocean  
690 sectors. Correlations significant at the 95% confidence level are indicated by the  
691 horizontal dashed lines. Positive lags indicate that the Pacific warm pool leads the Indian  
692 Ocean warm pool.

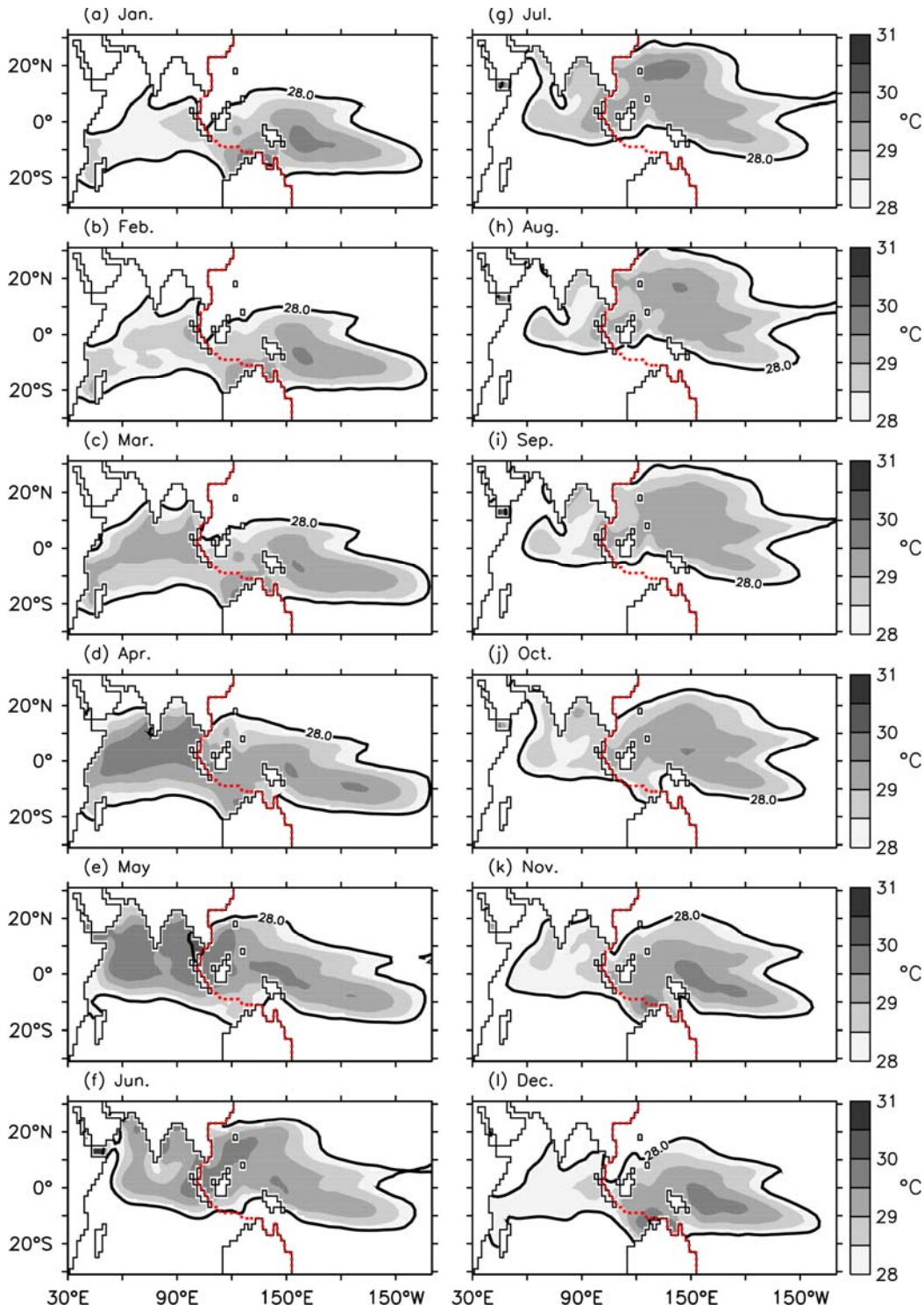
693 Table 1. Correlation coefficients of warm pool properties in the Pacific and Indian Ocean  
 694 sectors of the warm pool and the Niño3.4 index. The correlation coefficients are obtained  
 695 using whole monthly values and July-August-September (JAS) and December-January-  
 696 February (DJF) seasonally averaged values. Coefficients that are significant at 95%  
 697 according to student-t test are bold.  
 698

| Warm Pool Properties | Pacific Ocean |              |             | Indian Ocean |              |              |
|----------------------|---------------|--------------|-------------|--------------|--------------|--------------|
|                      | Monthly       | JAS          | DJF         | Monthly      | JAS          | DJF          |
| Size                 | <b>0.79</b>   | <b>0.75</b>  | <b>0.87</b> | <b>0.45</b>  | 0.21         | <b>0.64</b>  |
| Centroid, x          | <b>0.88</b>   | <b>0.89</b>  | <b>0.94</b> | <b>-0.35</b> | <b>-0.33</b> | <b>-0.39</b> |
| Centroid, y          | -0.15         | <b>-0.60</b> | 0.04        | 0.22         | 0.10         | <b>0.39</b>  |
| Mean SST             | 0.21          | -0.18        | <b>0.44</b> | <b>0.38</b>  | 0.18         | <b>0.58</b>  |
| Maximum SST          | 0.08          | -0.16        | 0.00        | 0.12         | -0.09        | 0.14         |



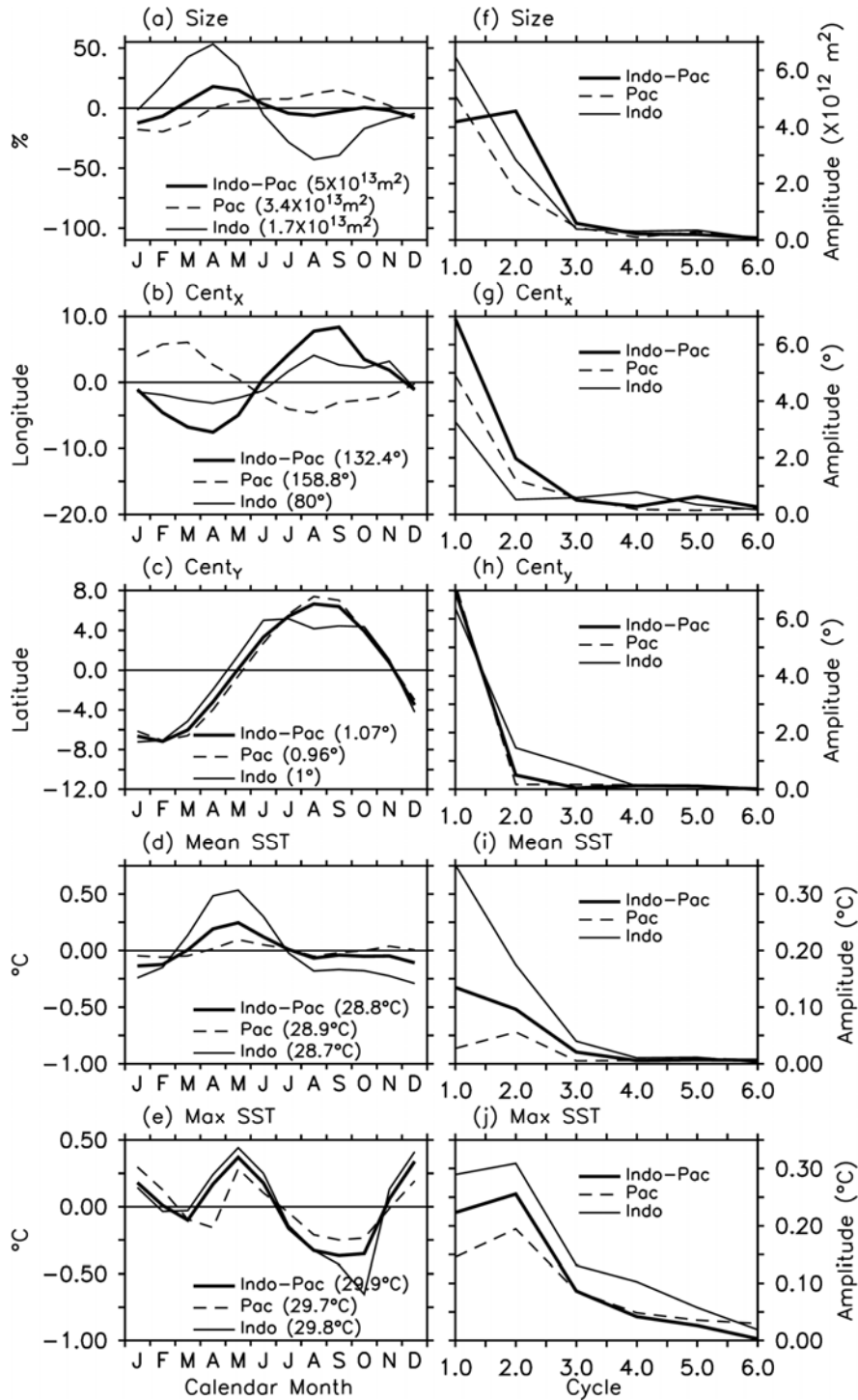
699

700 Figure 1. The seasonal evolution of the percentages of the Indo-Pacific warm pool in the  
 701 Pacific and Indian Ocean sectors.



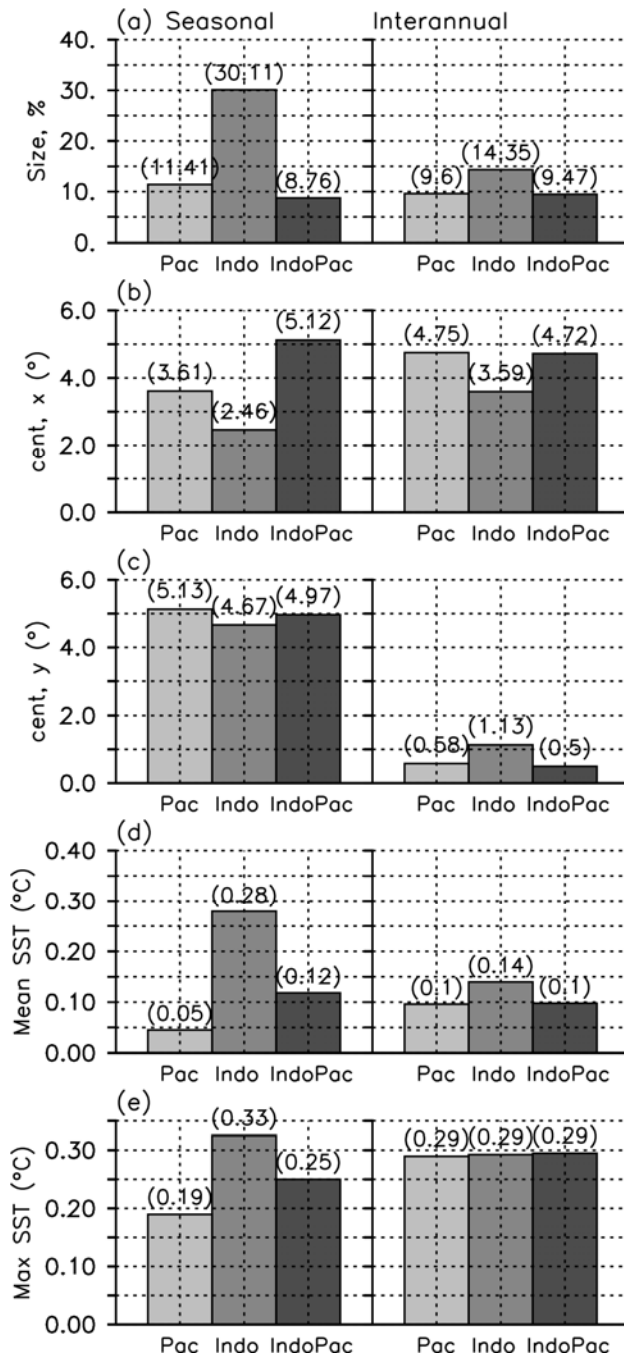
702

703 Figure 2. The monthly climatology of the Indo-Pacific warm pool SSTs. Values shown  
 704 are the monthly mean SSTs greater than 28°C; the threshold used to define the Indo-  
 705 Pacific warm pool. The boundary between the Pacific and Indian Ocean sectors of the  
 706 warm pool is indicated by red dashed line.



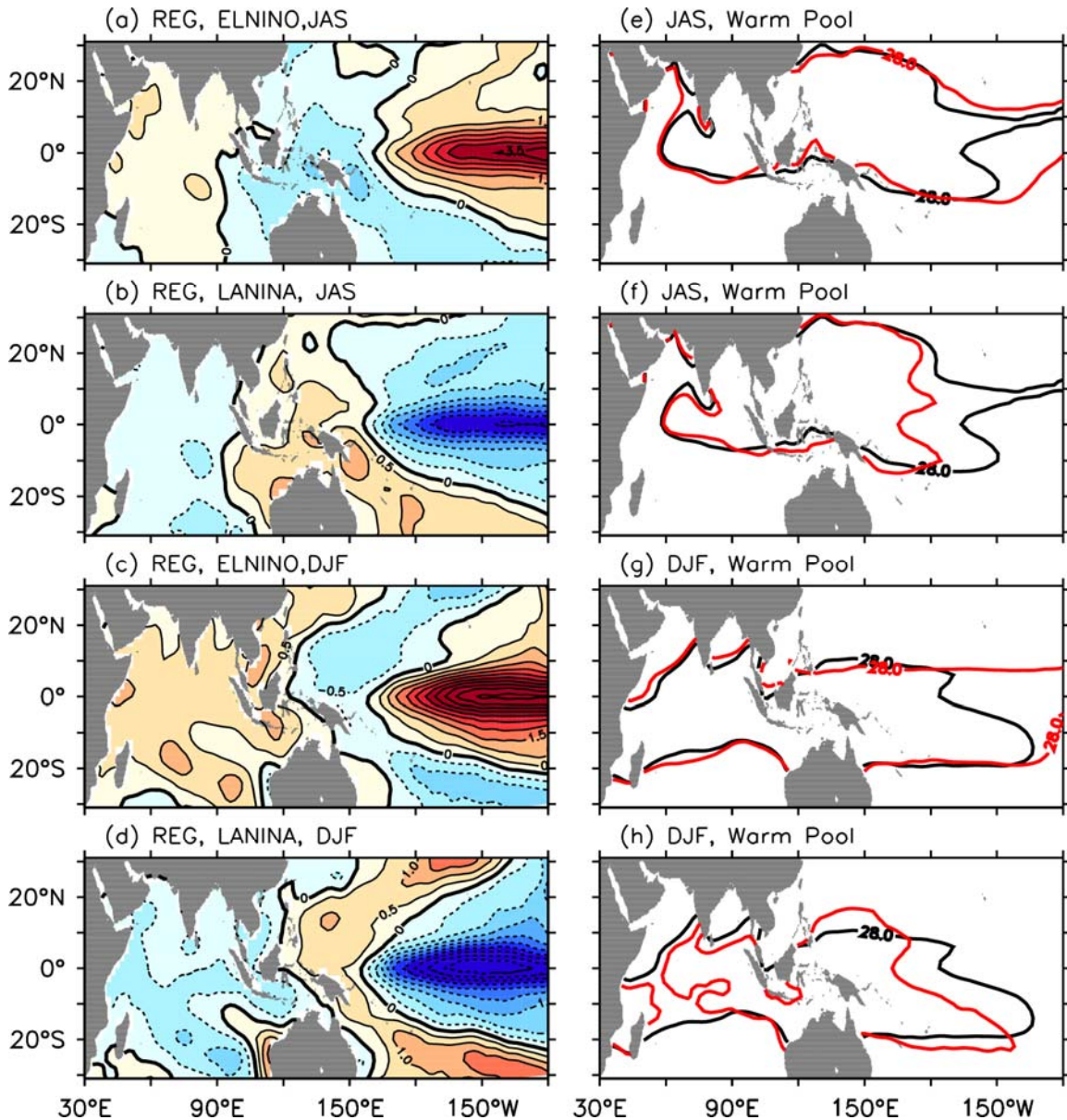
707

708 Figure 3. The seasonal cycle (left panels) and its harmonics (right panels) of warm pool  
 709 properties; (a, f) horizontal size, (b, g) the longitudinal displacement, (c, h) the latitudinal  
 710 displacement, (d, i) mean SST, and (e, j) maximum SST. Thick-solid lines represent  
 711 values for the Indo-Pacific warm pool, thin-dashed lines for the Pacific warm pool, and  
 712 thin-solid lines for the Indian Ocean warm pool.  
 713



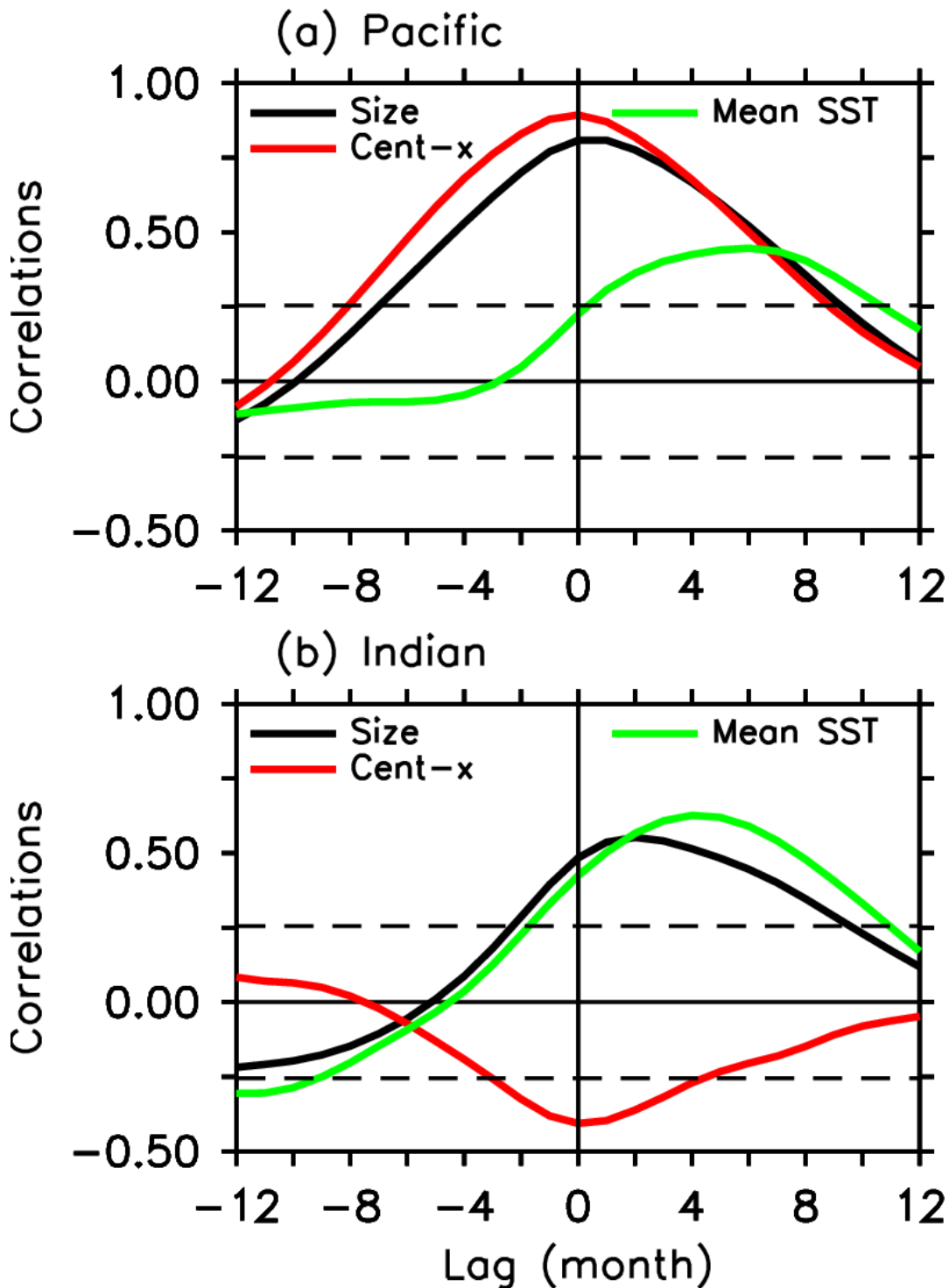
714  
715  
716  
717  
718  
719  
720  
721

Figure 4. Standard deviations of seasonal (left) and interannual (right) variability of (a) horizontal size, (b) mean SST, (c) maximum SST, (d) the longitudinal displacement, and (e) the latitudinal displacement for the Pacific and Indian Ocean sectors and the total warm pool. Values of the standard deviations are shown in parentheses on top of the bars.

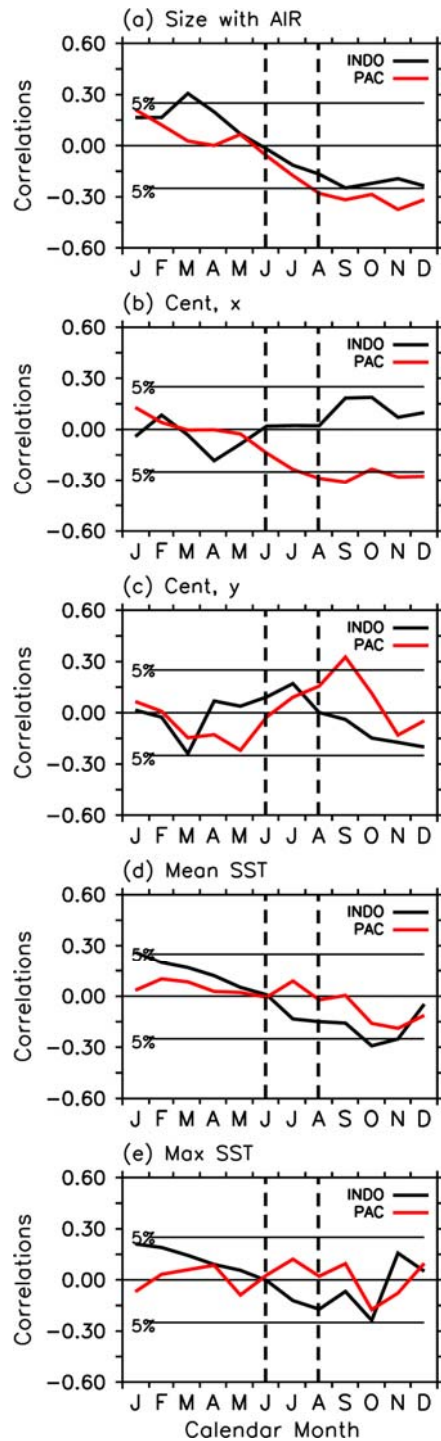


722  
 723  
 724  
 725  
 726  
 727  
 728  
 729  
 730

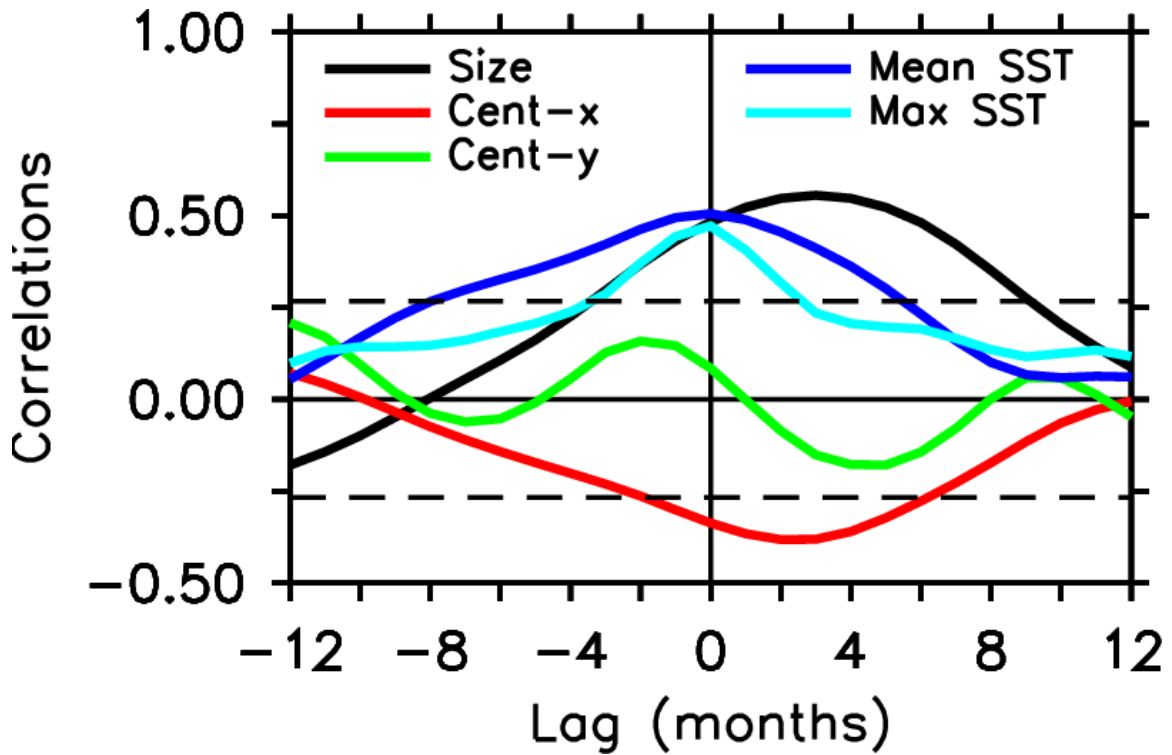
Figure 5. Spatial patterns of SST anomalies (left panels) and the warm pool (right panels). They are obtained separately for El Niño (a, c, e, g) and La Niña (b, d, f, h) phases and for JAS (a, b, e, f) and DJF (c, d, g, h) averaged values. The SSTA spatial patterns are produced by multiplying a four standard deviation (STD) of the Niño 3.4 index to the regression of the SSTA on the Niño3.4 SST index. The black 28°C isotherm of SST represents the JAS and DJF climatology and the red isotherm the sum of the climatology and regressed SSTA multiplied by four STD.



731  
 732 Figure 6. Lead-lag correlations between the Niño 3.4 indices and warm pool properties  
 733 for (a) the Pacific sector and (b) the Indian Ocean sector on interannual timescales. The  
 734 warm pool properties analyzed are the size (black), longitudinal displacement (red), and  
 735 mean SST (green). Positive lags indicate that the ENSO leads the warm pool properties.  
 736 Correlations significant at the 95% confidence level are indicated by the horizontal  
 737 dashed lines.



739  
 740 Figure 7. Correlations of the June-July-August All India rainfall (AIR) index with the  
 741 warm pool properties: (a) size, (b) longitudinal displacement, (c) latitudinal displacement,  
 742 (d) mean SST, and (e) maximum SST of the Pacific (red) and Indian Ocean (black) warm  
 743 pool. Correlations significant at the 95% confidence level are indicated by the horizontal  
 744 dashed lines.  
 745



746  
747

748 Figure 8. Lead-lag correlations of warm pool properties in the Pacific and Indian Ocean  
749 sectors. Correlations significant at the 95% confidence level are indicated by the  
750 horizontal dashed lines. Positive lags indicate that the Pacific warm pool leads the Indian  
751 Ocean warm pool.